

Topological Relaxation of a Shear-Induced Lamellar Phase to Sponge Equilibrium and the Energetics of Membrane Fusion

L. Porcar,^{1,3} W. A. Hamilton,² P. D. Butler,^{1,2} and G. G. Warr⁴

¹National Institute of Standards and Technology, Center for Neutron Research, Gaithersburg, Maryland 20899, USA

²Center for Neutron Scattering, Condensed Matter Sciences Division, Oak Ridge National Laboratory, Oak Ridge, Tennessee 37831, USA

³University of Maryland, College Park, Maryland 20742, USA

⁴School of Chemistry, University of Sydney, New South Wales 2006, Australia

(Received 25 May 2004; published 1 November 2004)

We report time-resolved small angle neutron scattering (t-SANS) measurements of the topological relaxation of Couette shear-induced stacked L_α lamellar states to their multiconnected isotropic L_3 sponge equilibrium phases in a surfactant bilayer membrane system. Comparison of this structural relaxation time to the interval between diffusive membrane contacts, as determined from dynamic light scattering or estimated from the shear rates required for L_α saturation, allows us to determine the activation energy barrier to the membrane fusion process reestablishing the solution channel handles that characterize the sponge phase.

DOI: 10.1103/PhysRevLett.93.198301

PACS numbers: 82.70.Dd, 47.20.Hw, 61.12.Ex, 87.16.Dg

While the fusion of membranes to create a solution passage is important in surfactant chemistry and crucial in cell biology, it also generally occurs relatively infrequently or against a confusing background of other phenomena or responses. Such is the case in the aptly named L_3 “sponge” phase, in which a single self-assembled surfactant bilayer spans a solution in a convoluted network of randomly directed passages [1]—topologically, handles in the membrane manifold. Despite this extended structure, these isotropic phases are typically highly fluid and show little or no response to applied shear, as passages can rapidly reorient or be created and destroyed in slight departures from equilibrium to relieve stresses on the membrane [2].

However, the L_3 phases occur in narrow regions of stability adjacent to those of the topologically distinct L_α lamellar phases, comparatively passage free stacked membranes in regular smectic order (Fig. 1). In light scattering measurements on “hyperswollen” $C_{12}E_5$ sponges at membrane volume fractions ϕ below 2%, Yamamoto and Tanaka [3] were able to demonstrate that applied shear could induce an L_3 to L_α transition. Recently we showed that adding an inert thickener, dextrose, to the brine solvent in the widely studied cetylpyridinium(CPCI)-hexanol membrane system significantly slowed membrane dynamics resulting in much stronger responses to applied shear $\dot{\gamma}$ [4,5]. The response depends upon a rescaled shear rate parameter, $\dot{\gamma}\eta_s/\phi^3$, where η_s is the viscosity of the solvent [6]. Over the range $10^7 < \dot{\gamma}\eta_s/\phi^3 < 4 \times 10^8 \text{ cP s}^{-1}$ CPCI-hexanol/dextrose-brine sponges shear-thin dramatically. Couette shear cell small angle neutron scattering (SANS) measurements showed that this rheological response corresponded to a gradual L_3 to stacked L_α transformation as membrane passages are disrupted, with full

L_α saturation alignment being achieved for $\dot{\gamma}\eta_s/\phi^3 \approx 2\text{--}4 \times 10^8 \text{ cP s}^{-1}$ [7].

Dextrose may be added to the brine solvent at volume fractions of up to 40% without significantly altering the equilibrium phase behavior of the CPCI-hexanol membranes, while increasing η_s from 1.1 to 16.3 cP. The corresponding increase in $\dot{\gamma}\eta_s/\phi^3$ makes the L_3 to L_α transition accessible at moderate dilutions (here $\phi = 3\%\text{--}7\%$) convenient for structural and rheological measurement. In the present work we take advantage of the well characterized response of this slowed system and the fact that on cessation of shear the relaxation of a shear-induced L_α state to the L_3 equilibrium phase requires that all of the passages destroyed by shear be reestablished. Thus this topological relaxation offers a strong clear signal of the fusion of membranes to (re)form passages.

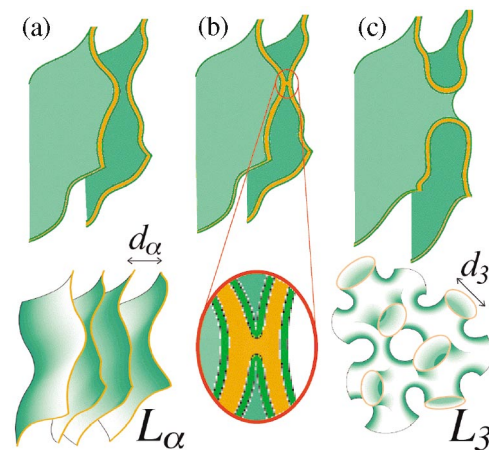


FIG. 1 (color). L_α and L_3 phase morphologies and characteristic sizes, and the stages of membrane passage formation discussed in the text.

Milner, Cates, and Roux (MCR) [8] noted that there are several stages in the formation of a passage or handle between bilayer membranes as required by L_α to L_3 relaxation: In Fig. 1(a) the separated membranes are brought together by diffusive motions; in 1(b) on contact some initial connecting structure must form; which then in 1(c) expands to form a solution passage. This is an activated process since it involves an energetically unfavorable intermediate state in which membranes are sharply curved and in close contact. Figure 1(b) shows one postulated intermediate state: a “stalk” merging proximal membrane monolayers, a form which has been used to estimate the mechanical free energy barriers which must be overcome or circumvented in intracellular or viral fusion [9–11].

Whatever the details of intermediate membrane fusion states, the activation energy barrier they represent E_F relates the topological relaxation time τ_R to the interval between membrane contacts τ_C as

$$\tau_R = \tau_C \exp[E_F/k_B T]. \quad (1)$$

Since the membranes are brought into contact by diffusion, τ_C can simply be determined from dynamic light scattering (DLS) measurements. Based on viscosity and birefringence measurements MCR estimated $E_F \sim 5k_B T$ (130 meV) and $\tau_R \sim 0.01$ s for typical dilute sponge samples, assuming $\eta_s \sim 1$ cP and $\phi \sim 3\%$. We note that this is much less than the hydrodynamic stopping time in our 1 mm gap Couette shear cell: $\tau_h \sim g^2 \rho / \eta$, where g is the gap and ρ and η are the fluid’s density and viscosity. For $g = 1$ mm, $\rho \sim 1$ g cm $^{-3}$, and $\eta \sim 1$ cP, we find $\tau_h \sim 1$ s. Our measurements rely on the fact that increasing η_s reduces τ_h , while slowing membrane dynamics by the same factor. All measurements were performed on high viscosity $\eta_s = 16.3$ cP 40 vol% dextrose-heavy brine L_3 samples for which the relative gain factor is over 200.

Even with the slowed dynamics of this system L_α to L_3 relaxation takes only a few seconds. To track this (for SANS) rapidly changing structural signal we employed the National Institute of Standards and Technology (NIST) SANS instrument NG7 in “time-slicing” mode: synchronizing time-binned SANS data acquisition with

the ORNL Couette SANS shear cell [12] to cycle through the process of shearing to a steady L_α state, stopping, and relaxing to L_3 equilibrium repeatedly to accumulate statistically significant measurements on much shorter time scales than is possible for individual runs [13]. Each cycle was begun with 20 s of Couette shear at a rescaled shear rate for that sample of $\dot{\gamma} \eta_s / \phi^3 \approx 3 \times 10^8$ cP s $^{-1}$, the center of the saturated L_α SANS signal range. The initial L_α signal was obtained by triggering data acquisition several bins before stopping the shear cell. That steady state conditions and full relaxation had been achieved was confirmed by simple comparison with time-sliced data acquired with the Couette cell running at the alignment rate or stopped.

Figure 2(a) shows some of the 0.1 s bin width t-SANS (time-resolved SANS) patterns for relaxation to L_3 equilibrium of an L_α state induced in a $\phi = 5\%$ sample by an applied Couette shear rate of $\dot{\gamma} = 2200$ s $^{-1}$ ($\dot{\gamma} \eta_s / \phi^3 \approx 2.9 \times 10^8$ cP s $^{-1}$) at 23 °C. This sample’s mass ratio of the hexanol and CPCl membrane components $h = 0.92$ is just on the hexanol rich side of the single phase stability region of L_3 for this system [5]. Measurements were performed with the incident beam radial and tangential to the Couette sample annulus yielding scattering patterns in the flow/vorticity (V, Z) and velocity gradient/vorticity ($\nabla V, Z$) planes, respectively. Initial patterns show the anisotropic scattering from the shear-induced L_α state at saturation. In the tangential patterns Bragg peaks at $Q_\alpha = 0.010$ Å $^{-1}$ indicate membranes stacked normal to ∇V (conventionally “c” alignment) at a smectic periodicity $d_\alpha = 630$ Å. In both geometries correlations on a much larger scale than the membrane separations give rise to some scattering near the beam stop. The Couette stop signal is issued at $t = 0$ and the shear cell comes to a full stop in the next half second, over which time this low Q scattering disappears. Over the next two seconds the lamellar Bragg signal decays in the tangential scattering patterns and a ring of scattering appears for both geometries indicating the reestablishment of the isotropic L_3 structure. The correlation ring at $Q_3 = 0.008$ Å $^{-1}$ corresponds to a mean L_3 passage size d_3 of 790 Å—about 25% larger than d_α . (The same scale

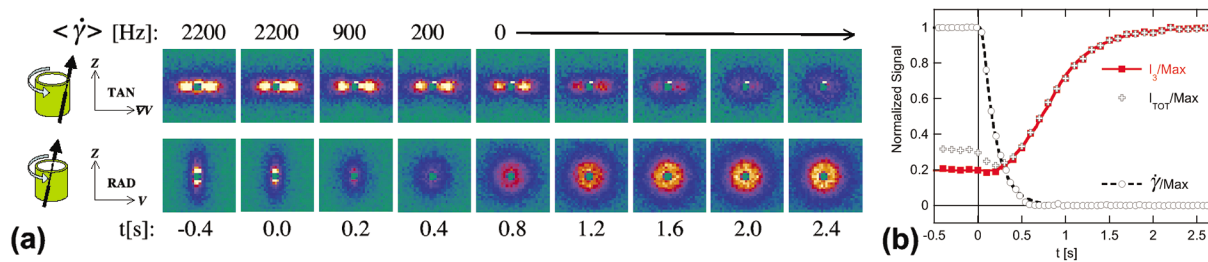


FIG. 2 (color). Topological relaxation for $\phi = 5\%/h = 0.92$ CPCl-hexanol in 40 vol% dextrose-heavy brine: (a) 0.1 s time-binned Couette SANS patterns in radial and tangential geometry. For $t < 0$ applied shear rate $\dot{\gamma} = 2200$ s $^{-1}$, tangential data Bragg peaks indicate “c” aligned L_α steady state. After $t = 0$ isotropic L_3 equilibrium is reestablished over about 2 s. (b) Normalized signals of applied shear rate $\dot{\gamma}/\text{Max}$; total radial scattering intensity $I_{\text{TOT}}/\text{Max}$; and (in red) scattering from the region of the sponge correlation peak I_3/Max , with line fit for $\tau_R = 0.40 \pm 0.08$ s.

ratio is seen between equilibrium L_3 and L_α phases at the same ϕ .)

The intensity of the isotropic L_3 scattering is directly related to the reformation of the handles between adjacent membrane sheets and thus to τ_R . Figure 2(a) shows that the clearest signal of this intensity is available from the radial scattering patterns. In the tangential patterns the decaying L_α Bragg peak signal overwhelms the initial appearance of the L_3 correlation ring signal. In radial patterns the L_α state offers no competing signal near the L_3 correlation peak and the low Q scattering observed at L_α saturation extends over a smaller region and only in the Z direction.

Figure 2(b) shows integrated SANS signals for the $\phi = 5\%/h = 0.92$ radial relaxation series as function of time, both for the full detector and after excluding the low Q region, as $I_{\text{TOT}}/\text{Max}$ and I_3/Max , respectively, for convenient display signals have been normalized to their maximum values. Also shown is $\dot{\gamma}/\text{Max}$, from the tachometer signal from the Couette cell motor as the cells rotating cup comes to a stop from the alignment shear rate $\dot{\gamma} = 2200 \text{ s}^{-1}$. The fit to $\dot{\gamma}/\text{Max}$ indicates an effective exponential decay time for the applied shear rate $\tau_{\dot{\gamma}} \approx 0.15 \text{ s}$, about twice the estimated hydrodynamic stopping time $\tau_h \sim 0.07 \text{ s}$. In the full detector signal the falloff of the low Q scattering as the Couette cell stops shows as an initial dip in the total signal before the rise due to the correlation ring signal of the reforming sponge topology. When this signal is subtracted in I_3/Max the initial growth of the L_3 signal is seen to begin at a delay of $\sim 0.2 \text{ s}$ from the initial fall in $\dot{\gamma}$ —a consequence of the time required for $\dot{\gamma}\eta_s/\phi^3$ to fall below the minimum value for L_α saturation $2 \times 10^8 \text{ cP s}^{-1}$ from the alignment value of $2.9 \times 10^8 \text{ cP s}^{-1}$. The fit to this data taking into account the time resolution of the t-SANS measurement $\sigma_t \approx 0.2 \text{ s}$ (0.1 s SANS binning, $\tau_h \sim 0.07 \text{ s}$, and $\tau_{\dot{\gamma}} \approx 0.15 \text{ s}$) indicates simple exponential decay of the rate of growth of the L_3 signal as the topology is reestablished with a relaxation time $\tau_R = 0.40 \pm 0.08 \text{ s}$.

DLS measurements were performed in homodyne mode after samples were filtered ($0.2 \mu\text{m}$ pore size) and maintained at 23°C for several hours. Observed time scattering correlations were stretched exponential $\exp[-2(\Gamma t)^\beta]$ with exponent $0.7 < \beta < 0.8$, consistent with theoretical predictions of diffusion behavior in softer membrane systems such as ours [14] and measurements on a variety of similar systems [15–17]. The characteristic relaxation frequency Γ was proportional to Q^2 , consistent with a simple diffusion process [18]. No Q^3 dependence was observed for even our most dilute samples, indicating that we are probing membranes incorporated within an extended structure rather than observing the undulation dynamics of isolated fragments. Hence $\Gamma = DQ^2$, where D is the cooperative membrane diffusion coefficient. The values of D were proportional to ϕ for each sample.

The time required for diffusion to bring together membranes from a mean separation d may be estimated as $1/DQ^2$, where $Q \equiv 2\pi/d$. In determining τ_C we used the Q value of the L_α Bragg peaks. Since both D and $Q_\alpha \equiv 2\pi/d_\alpha$ are proportional to ϕ we find that $\tau_C[Q_\alpha]$ is proportional to ϕ^{-3} . As might be expected this is consistent with the shear response scaling of this system. Further, the values of τ_C coincide closely with the times that are indicated (as $1/\dot{\gamma}$) by considering that the shear-induced L_α saturation plateau range, $\dot{\gamma}\eta_s/\phi^3 \approx 2\text{--}4 \times 10^8 \text{ cP s}^{-1}$, represents a complete frustration of membrane passage creation (Shaded regions in Figs. 3 and 4).

In Fig. 3 we show τ_R and τ_C determined for parallel sample series at varying ϕ , from 3% to 10%, maintaining a constant hexanol to CPCI mass ratio $h = 0.92$. For this dilution series there is no significant change in the intrinsic membrane properties [19]: the bending modulus κ , which governs the dynamics of membrane fluctuations, or the Gaussian curvature (or saddle-splay) modulus $\bar{\kappa}$. Values of τ_C derived from DLS are shown as open circles and most τ_R from t-SANS as solid squares. However, for the fastest topological relaxation ($\phi = 7\%/h = 0.92$) a downward solid triangle indicates a measurement near the resolution limits of the t-SANS technique as implemented ($\sim 0.1 \text{ s}$) which strictly represents only an upper limit to τ_R . Consistent with the Arrhenius relationship Eq. (1) we found that τ_R , like τ_C , scales as ϕ^{-3} , with the ratio $\tau_R/\tau_C \approx 820$, indicating a constant activation energy $E_F \approx 6.7k_B T$ (170 meV). This strongly suggests that the intermediate fusion structures which raise this barrier to reestablishing the sponge phase handles do not vary with or gain significant energetic impetus from structural organization or dynamics on the length and curvature scales characteristic of these L_3 and shear-induced L_α states.

Variation of the membrane composition ratio h directly controls the phase behavior in this system by altering $\bar{\kappa}$, which enters the Canham-Helfrich Hamiltonian for

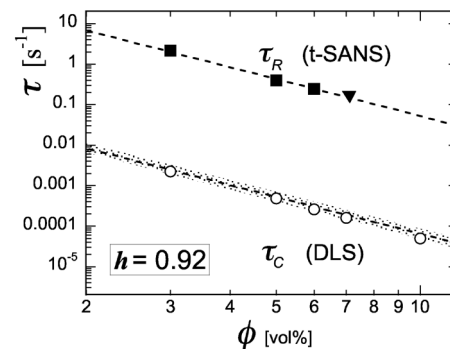


FIG. 3. Membrane contact intervals, τ_C , and topological relaxation times, τ_R , versus membrane volume fraction ϕ at constant hexanol to CPCI membrane composition ratio, $h = 0.92$. Dashed lines are ϕ^{-3} . Shaded regions indicate $1/\dot{\gamma}$ for the shear-induced L_α saturation plateau $\dot{\gamma}\eta_s/\phi^3 \approx 2\text{--}4 \times 10^8 \text{ cP s}^{-1}$.

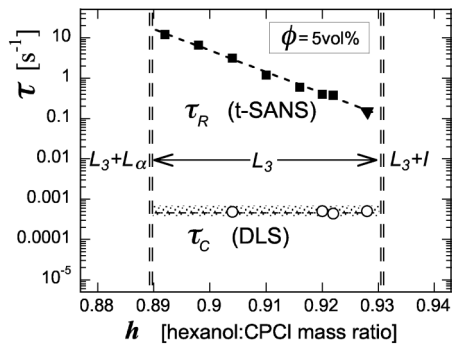


FIG. 4. Membrane contact intervals, τ_C , and topological relaxation times, τ_R , versus hexanol to CPCI membrane composition ratio h for $\phi = 5\%$ samples. Shaded region is $1/\dot{\gamma}$ over the shear-induced L_α saturation plateau.

membranes [20] as an energy contribution $dE_G = \bar{\kappa}GdA$, where G is the Gaussian curvature over the area element dA . From the Gauss-Bonnet theorem the integral of G over a manifold is a simply function of the topology with a contribution -4π from each handle, so each represents an energy difference of $-4\pi\bar{\kappa}$, with positive values of $\bar{\kappa}$ favoring the formation of the L_3 phase [21]. At a constant $\phi = 5\%$ we performed t-SANS measurements over a range of h from 0.892 to 0.928, across the L_3 single phase stability region, from a boundary with a biphasic $L_3 + L_\alpha$ region at lower h to an upper boundary with a coexistence region of L_3 domains in excess solvent ($L_3 + I$). The increase in $\bar{\kappa}$ with h reflected in the increased intrinsic curvature of this phase sequence may be expected to lower the energy barrier to the formation of highly curved intermediate structures.

This is confirmed in the log-lin plot Fig. 4 which shows measurements of τ_R versus h over the width of the L_3 phase region at a constant $\phi = 5\%$. We see that τ_R decays exponentially with increasing h . (Here again the fastest relaxation, for $\phi = 5\%/h = 0.928$, is resolution limited.) Meanwhile, a parallel DLS series shows that τ_C is constant over this range, since changing h has little effect on κ which controls the dynamical motions that bring membranes into contact [14,19]. From Eq. (1) we find that E_F varies linearly with h and therefore $\bar{\kappa}$ (since the total change in h over the L_3 phase region is only 4%): falling from $10.3k_B T$ (260 meV) for $h = 0.892$ down to $5.8k_B T$ (150 meV) for $h = 0.928$, a decrease of $1.2k_B T$ (30 meV) for each 1% increase in h [22].

In conclusion, we note that the values of E_F determined by this method on our viscously tuned system agree quite well with the values indirectly estimated by MCR [8], giving some confidence in its validity [23]. It is also very attractive to consider applying the technique to biological or biomimetic membrane fusion, if a lipid bilayer system with a suitable relaxation mode could be identified or engineered.

We acknowledge the following: Discussions with G. Porte and R. Prud'homme; J. P. Fluxench on Fig. 1; D. Glandon and B. Taylor on the ORNL Couette SANS cell;

B. Greenwald on NG7 and Charlie Glinka's leadership of the NIST SANS group; help from M. Yethiraj and M. Lumsden; and the Australian Nuclear Science and Technology Organization and the Australian Research Council (G.G.W.). NG7 is operated by NIST, U.S. Department of Commerce (with funding from the U.S. National Science Foundation under Agreement No. DMR-9986442). This Research was sponsored by the Laboratory Directed Research and Development Program of ORNL (managed by UT-Battelle, LLC for the U.S. Department of Energy under Contract No. DE-AC05-00OR22725).

- [1] G. Porte, *Curr. Opin. Colloid Interface Sci.* **1**, 345 (1996), and references therein.
- [2] P. Snabre and G. Porte, *Europhys. Lett.* **13**, 641 (1990).
- [3] J. Yamamoto and H. Tanaka, *Phys. Rev. Lett.* **77**, 4390 (1996).
- [4] L. Porcar *et al.*, *Phys. Rev. Lett.* **89**, 168301 (2002).
- [5] L. Porcar *et al.*, *Langmuir* **19**, 10779 (2003).
- [6] This scaling was first predicted by M. E. Cates and S. T. Milner, *Phys. Rev. Lett.* **62**, 1856 (1989).
- [7] For $\dot{\gamma}\eta_s/\phi^3 > 4 \times 10^8 \text{ cPs}^{-1}$ the L_α signal "collapses" [see S. Ramaswamy, *Phys. Rev. Lett.* **69**, 112 (1992)] and strong scattering emerging at small scattering vectors indicates a larger scale ordering [4,5].
- [8] S. T. Milner, M. E. Cates, and D. Roux, *J. Phys. (France)* **51**, 2629 (1990).
- [9] D. P. Siegel, *Biophys. J.* **65**, 2124 (1993); **76**, 291 (1999).
- [10] R. Jahn and H. Grubmuller, *Curr. Opin. Cell Biol.* **14**, 488 (2002); L. K. Tamm, J. Crane, and V. Kiessling, *Curr. Opin. Struct. Biol.* **13**, 453 (2003).
- [11] L. Yang and H. Huang, *Science* **297**, 1877 (2002).
- [12] L. Porcar *et al.*, *Rev. Sci. Instrum.* **73**, 2345 (2002).
- [13] W. A. Hamilton *et al.*, *Phys. Rev. E* **60**, 1146(R) (1999); L. Porcar *et al.*, *Physica (Amsterdam)* **350B**, e963 (2004).
- [14] A. G. Zilman and R. Granek, *Chem. Phys.* **284**, 195 (2002).
- [15] E. Freyssingas *et al.*, *J. Phys. II (France)* **7**, 913 (1997).
- [16] Y. Kimura *et al.*, *Mol. Cryst. Liq. Cryst. A* **332**, 3069 (1999).
- [17] S. Komura *et al.*, *Phys. Rev. E* **63**, 041402 (2001).
- [18] G. Porte *et al.*, *J. Phys. II (France)* **1**, 1101 (1991).
- [19] G. Porte, *J. Phys. Condens. Matter* **4**, 8649 (1992). We neglect the slow variation (as $\ln\phi$) of entropic corrections.
- [20] P. B. Canham, *J. Theor. Biol.* **26**, 61 (1970); W. Helfrich, *Z. Naturforsch. C* **28**, 693 (1973).
- [21] W. Helfrich, *J. Phys. Condens. Matter* **6**, A79 (1994).
- [22] Assuming proximal monolayer stalk intermediates [Fig. 1(b)] and Canham-Helfrich Hamiltonian validity at high curvatures, the Gaussian curvature energy would be $-4\pi\bar{\kappa}_m$, where $\bar{\kappa}_m \approx \bar{\kappa}/2$ is the monolayer curvature modulus [1]. The change in E_F across the L_3 region would correspond to a increase in $\bar{\kappa}_m$ of $0.1k_B T$ (2.5 meV) for each 1% increase in h , and about twice that for $\bar{\kappa}$.
- [23] We note that a similar interpretation was applied to two exponential DLS correlation signal observed in a micro-emulsion system by U. Peter, D. Roux, and A. K. Sood, *Phys. Rev. Lett.* **86**, 3340 (2001).